

ESR of quasi-two-dimensional antiferromagnet with triangular lattice CuCrO_2

A. M. Vasiliev, L. A. Prozorova, and L. E. Svistov*

P. L. Kapitza Institute for Physical Problems RAS, 119334 Moscow, Russia

V. Tsurkan

Experimental Physics V, EKM, University of Augsburg, D-86159 Augsburg, Germany

V. Dziom, A. Shuvaev, Anna Pimenov, and A. Pimenov

Institute of Solid State Physics, Vienna University of Technology, A-1040 Vienna, Austria

(Dated: June 6, 2019)

Using electron-spin-resonance (ESR) technique we investigate the magnetic structure of CuCrO_2 , quasi-two-dimensional antiferromagnet with weakly distorted triangular lattice. Resonance frequencies and the excitation conditions in CuCrO_2 at low temperatures are well described in the frame of cycloidal spin structure, defined by two susceptibilities parallel and perpendicular to the spin plane (χ_\perp and χ_\parallel) and by a biaxial crystal-field anisotropy. In agreement with the calculations, the character of the eigenmodes changes drastically at the spin-flop transition. The splitting of the observed modes can be well attributed to the resonances from different domains. The domain structure in CuCrO_2 can be controlled by annealing of the sample in magnetic field.

PACS numbers: 75.50.Ee, 76.60.-k, 75.10.Jm, 75.10.Pq

I. INTRODUCTION

Magnetic materials with frustrated exchange interactions are one of the attractive issues in modern solid state physics. In these materials unconventional magnetic orders appear as a subtle balance of exchange energies and they are often governed by much weaker interactions or fluctuations. Such frustrated systems are known in nature for quasi-one-dimensional, quasi-two-dimensional and three-dimensional cases. For one(two)-dimensional magnets the interactions within the chain (plane) are much larger than the coupling of spins from different chains (planes).

Magnetic properties of an antiferromagnet on a regular triangular planar lattice have been intensively studied theoretically.¹⁻⁶ The ground state in the Heisenberg and XY-models is a “triangular” planar spin structure with three magnetic sublattices arranged by 120° apart. After neutron scattering experiments⁷ CuCrO_2 was for a long time ascribed to magnets with regular triangular structure and with 120-degree spin arrangement in the planes. A disorder caused by frustration of the inter-plane exchange bonds was also suggested. Recent neutron scattering investigations⁸ in CuCrO_2 single crystals detected a three dimensional magnetic order with incommensurate wave vector that slightly differs from the wave vector of a commensurate 120-degrees structure. The magnetic ordering is accompanied by a simultaneous crystallographic distortion⁹ of the regular triangular lattice and by the appearance of an electrical polarization. The electric polarization in CuCrO_2 can be influenced by comparatively weak magnetic field. Microscopic mechanism of this complex magneto-elastic transition is not well understood and is a subject of actual investigations.

Electron spin resonance (ESR) technique is a powerful tool to investigate magnetically ordered states of mat-

ter. The high field ESR in CuCrO_2 was investigated in Ref. [10]. Although the flop of the cycloidal plane was detected at $H_c = 5.3$ T, many of important issues such as the polarization analysis of the excitation conditions and the separation of the contributions from different domains remain open. In this work the detailed magnetic and domain dynamics of quasi-two dimensional antiferromagnet with the triangular lattice CuCrO_2 has been investigated using ESR technique in a broad frequency range.

II. CRYSTAL STRUCTURE AND MAGNETISM IN CuCrO_2

CuCrO_2 crystallizes in a delafossite structure (space group $R\bar{3}m$) with the following hexagonal unit cell parameters at room temperature: $a = 2.98$ Å, $c = 17.11$ Å. The unit cell of CuCrO_2 contains three formula units. Chromium ions occupy the positions $(0; 0; 1/2)$, $(1/3; 2/3; 1/6)$, $(2/3; 1/3; 5/6)$ in the crystal cell (see Fig. 1) and Cu^+ ions occupy the positions $(0; 0; 0)$, $(1/3; 2/3; 2/3)$, $(2/3; 1/3; 1/3)$ (Ref. [11]). Magnetic Cr^{3+} ions ($S = 3/2$) form a triangular lattice in the ab -planes. Adjacent planes are separated by nonmagnetic copper ions along the c -axis. At temperatures above the Néel temperature ($T > T_N \approx 24$ K) the triangular lattice is regular. In the magnetically ordered state the triangular lattice is distorted, such that one side of the triangle becomes slightly smaller than two other sides: $\Delta a/a \simeq 10^{-4}$ (Ref. [12]).

According to neutron diffraction experiments at low temperatures a spiral incommensurate spin structure with a wave vector $\mathbf{q}_{ic} = (0.329, 0.329, 0)$ is established^{8,13,14}. The cycloidal rotation of the magnetic mo-

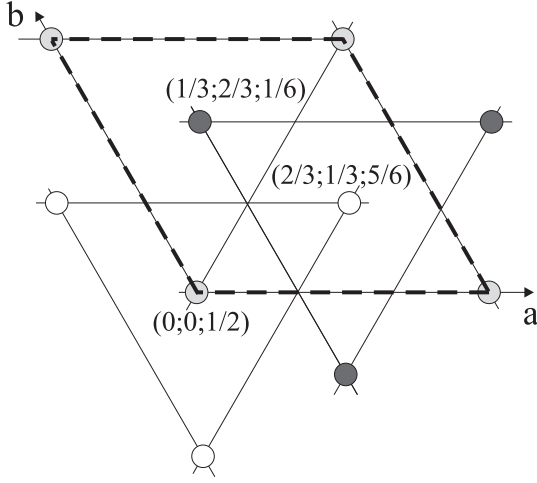


FIG. 1: Crystal structure of CuCrO_2 in projection on the ab -plane. The positions of Cr^{3+} ions are marked by circles. The crystal cell is outlined with dashed line.

ments \mathbf{M}_i of Cr^{3+} ions may be written as:

$$\mathbf{M}_i = M_1 \mathbf{e}_1 \cos(\mathbf{q}_{ic} \cdot \mathbf{r}_i + \psi) + M_2 \mathbf{e}_2 \sin(\mathbf{q}_{ic} \cdot \mathbf{r}_i + \psi), \quad (1)$$

where \mathbf{e}_1 and \mathbf{e}_2 are two perpendicular unit vectors determining the spin plane orientation with the normal vector $\mathbf{n} = \mathbf{e}_1 \times \mathbf{e}_2$, and ψ is an arbitrary phase. The values of the magnetic components (M_1 , M_2) depend on the arrangement of the spiral plane with respect to the crystal axes. For zero magnetic field \mathbf{e}_1 is parallel to $[001]$ with $M_1 = 2.2(2) \mu_B$ and \mathbf{e}_2 is parallel to $[1\bar{1}0]$ with $M_2 = 2.8(2) \mu_B$, respectively (Ref. [13]). The difference between M_1 and M_2 reflects the ellipticity of the helix.

According to the results of inelastic neutron scattering¹⁴ the interaction is strongest in the trigonal plane between the nearest Cr^{3+} ions with the exchange constant $J_{ab} = 2.3$ meV. The inter-plane interaction is frustrated and at least one order of magnitude weaker than the in-plane interaction. The nature of the incommensurability of magnetic structure is not clear at present. The value of the incommensurate vector $(0.329, 0.329, 0)$ is very close to the vector of the regular triangle structure $(1/3, 1/3, 0)$ and can be explained by weak interactions. For example, the incommensurability can be influenced by small difference of in-plane interactions of distorted triangles: $J_{ab}/J'_{ab} = -2 \cos(2\pi q_{ic}) \approx 1.05$. Here J'_{ab} is the exchange interaction along the nonequal edges of the distorted triangle. Alternatively, the observed incommensurability can be explained by joint influence of the inter-plane and the next-nearest intra-plane interactions¹⁴.

The plane of the spin cycloid in CuCrO_2 is perpendicular to one side of the triangle¹⁵. Accordingly, three equivalent magnetic domains coexist in the ordered state. Such arrangement of the spin plane is in agreement with a strong “easy axis” single ion anisotropy along the c -axis as obtained from inelastic neutron scattering experiments¹⁴. Therefore, the magnetic domains

are characterized by both, the distortion of the triangular plane parallel to $[100]$, $[010]$, $[110]$ and the orientation of the cycloidal spin plane with the normal vector $\mathbf{n}_{1,2,3} \parallel [100]$, $[010]$, $[110]$, respectively. Such domains will be referred in the text as $[100]$, $[010]$ and $[110]$ domains.

The orientation of the spin plane with respect to triangular plane is defined by a weak in-plane anisotropy and can be influenced by moderate external magnetic field. For $\mathbf{H} \parallel [1\bar{1}0]$ the spin reorientation transition was observed at 5.3 T.¹⁰

III. EXPERIMENTAL DETAILS

Single crystals of CuCrO_2 were grown by a flux method with Bi_2O_3 solvent. Powder X-ray diffraction measurements of the single crystals did not show any impurity phases. The crystals had a platelet shape (approximately $3 \times 3 \times 0.5$ mm³) with the large surface perpendicular to the hexagonal c -axis.

Initial polycrystalline CuCrO_2 samples were prepared by solid-state reaction from a stoichiometric mixture of CuO and Cr_2O_3 ¹⁶. The mixture was pressed into pellets and sintered at 1000°C for 40 hours in air. This procedure was repeated after intermediate grinding for 40 h at the same temperature.

The ESR experiments were performed with a transmission-type spectrometer using various resonators in the frequency range $14 < \omega/2\pi < 140$ GHz. The superconducting solenoid has provided magnetic fields up to 8 T.

The high frequency branch of the spectra was studied using the quasi-optical technique^{17,18}. In the case of magnetic excitations the transmission through the sample can be obtained as a function of either temperature, frequency, or external magnetic field¹⁹. Due to well-defined polarization of the electromagnetic radiation the orientation of the ac magnetic field is also known in addition to the direction of the static field. For the present study the following ranges of external parameters have been utilized: $300 < \omega/2\pi < 450$ GHz, $0 < H < 7$ T, and $2 < T < 30$ K. The spectra have been analyzed using Fresnel optical expressions for the transmission of a plane-parallel sample assuming Lorentzian form of the complex magnetic permeability:

$$\mu^*(H) = 1 + \frac{\Delta\mu H_0^2}{H_0^2 - H^2 - iHg}. \quad (2)$$

Here $\Delta\mu$, H_0 , and g are magnetic contribution, resonance field and resonance width, respectively.

IV. RESULTS

Lower panels of Figs. 2, 3 show magnetic field dependencies of the ESR signal in CuCrO_2 at different radiation frequencies. These curves were obtained for the magnetic field directed parallel (Fig. 2) and perpendicular

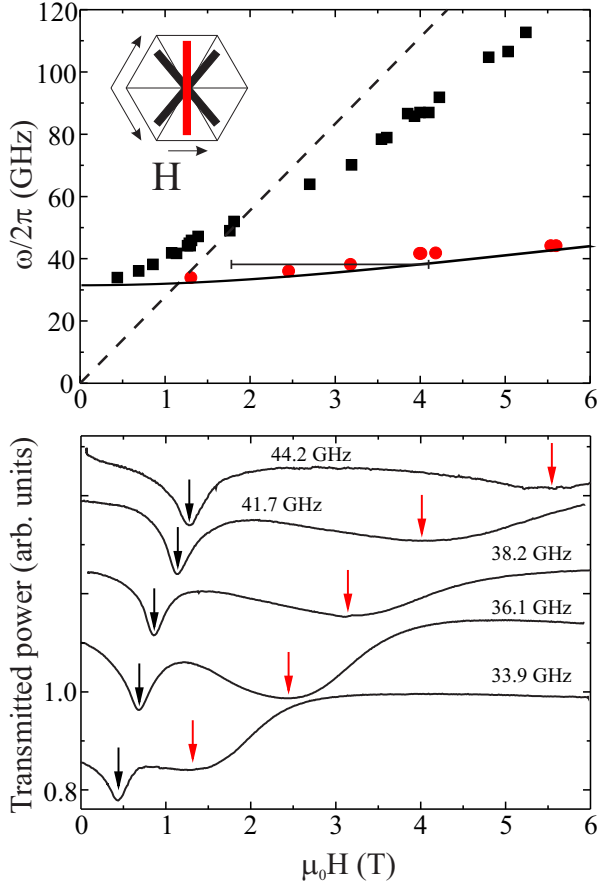


FIG. 2: (color online) Upper panel: Magnetic field dependence of the ESR frequencies for CuCrO₂ single crystal. Magnetic field is directed parallel to one side of triangular structure: $H \parallel [110]$. Red circles can be attributed to the ESR from the domains with the distorted side aligned along the $[110]$ direction. The black squares corresponds to resonances from the domains with the distortions along $[100]$ and $[010]$, respectively. The geometry of the experiment is shown in the inset. Solid line shows the calculated $\omega(H_{res})$ within the model discussed in the text. The dotted line corresponds to a paramagnetic mode with g -factor equal 2. Lower panel: Examples of ESR absorption spectra at $T = 4.2$ K. Black and red arrows mark the absorption modes corresponding to the black and red symbols on the top panel.

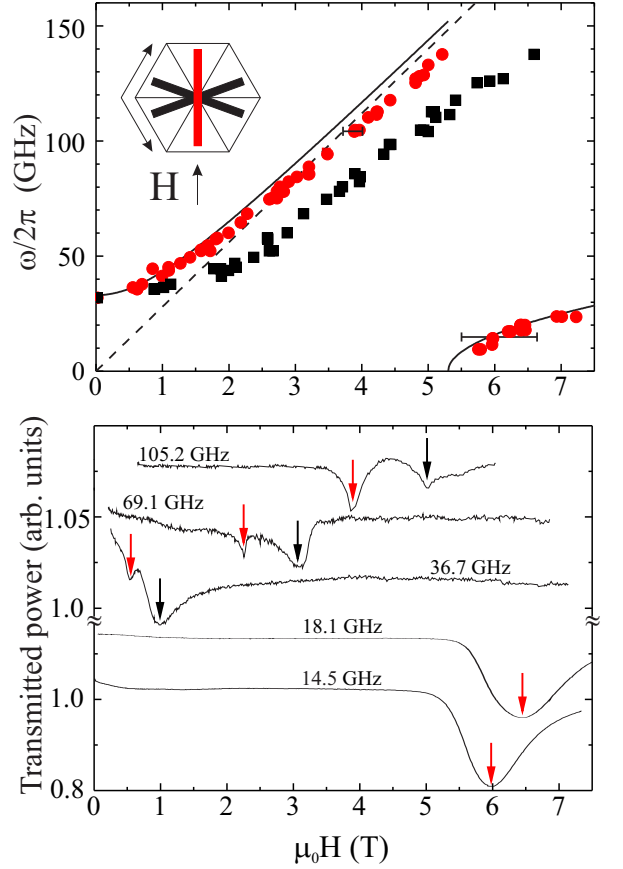


FIG. 3: (color online) Upper panel: ESR frequencies in CuCrO₂ for magnetic field directed perpendicular to one side of triangular structure: $H \parallel [\bar{1}10]$. Red circles can be attributed to the modes from the domains with the distorted side aligned along $[110]$. The black squares corresponds to resonances from the domains with distortions along $[100]$ and $[010]$. Orientations of the crystallographic axes, applied field and spin planes of three domains are shown in the inset. Solid lines show the calculated $\omega(H_{res})$ dependences within the model discussed in the text. The dotted line corresponds to a paramagnetic mode with $g = 2$. Lower panel: Examples of ESR absorption lines at $T = 4.2$ K. Black and red arrows mark the absorption lines corresponding to the black and red symbols on the top.

(Fig. 3) to one side of the triangular lattice. Corresponding frequencies of the resonance field (H_{res}) are shown in the upper panels. Since the distortion of the triangle at $T < T_N$ can happen along arbitrary side of a triangle structure, we can expect three absorption lines from the three domains shown in the insets. For field directions parallel and perpendicular to one side of the triangular structure, two of three domains will be in equivalent resonance conditions.

Red symbols in Figs. 2, 3 correspond to domain with the distortion along the $[110]$ direction. Black and blue symbols throughout this paper correspond to the resonances from two other domains with distortions along the $[100]$ or $[010]$ directions. The $\omega(H_{res})$ dependence

measured for $\mathbf{H} \parallel [\bar{1}10]$ direction for $[110]$ domain (red symbols on Fig. 3) shows abrupt softening of one resonance frequency at $H_c \approx 5.3$ T. This field corresponds to the spin reorientation transition observed in Ref. [10]. The spin reorientation can only be observed in the geometry with the static magnetic field applied along the plane of one of the spin cycloids. If magnetic field is applied perpendicular to the cycloidal plane (as in Fig. 2) then two other domains will rotate continuously and no spin reorientation occurs.

Angular dependence of the resonance fields measured at $\omega/2\pi = 36.1$ GHz is shown in Fig. 4. Magnetic field is rotated within the plane of the triangular structure, i.e. within the (001) -plane. Red circles, black squares, and

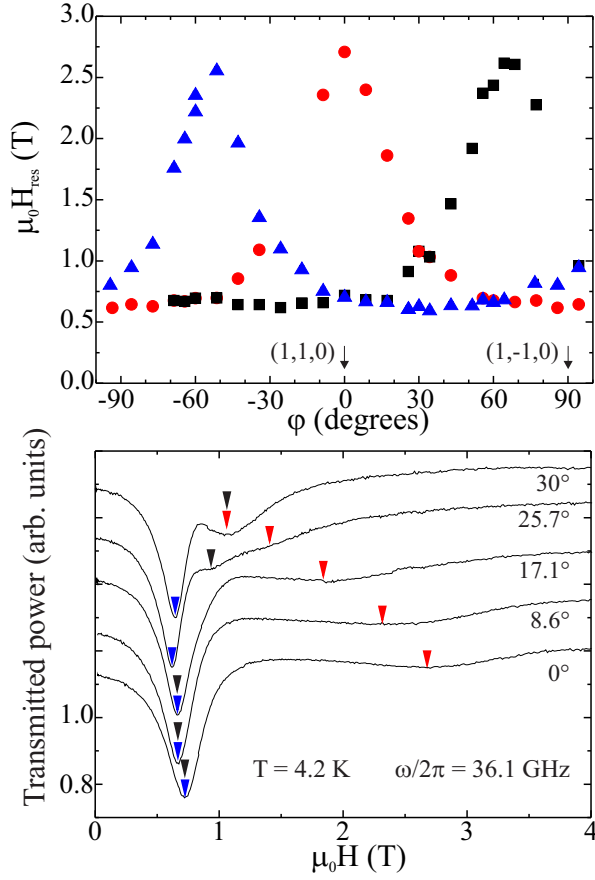


FIG. 4: (color online) Upper panel: Angular dependence of the resonance fields for static magnetic field rotated within the plane of the triangular structure (001) and at $\omega/2\pi = 36.1$ GHz. Red circles, black squares, and blue triangles correspond to the ESR modes from three domains with distortions along $[110]$, $[100]$, and $[011]$, respectively. Lower panel: Examples of the ESR absorption spectra for different directions of the external magnetic field.

blue triangles in the $\omega(H)$ spectra and red, black and blue arrows at the absorption lines from the lower panel can be attributed to the resonances from three magnetic domains. The angular dependence of resonance field (H_{res}) from every domain has 180 degrees periodicity. The angles at which the resonance fields of different modes coincide follow a triangular geometry. The spectrum in the lower panel of Fig. 4 taken at $\varphi = 0^\circ$ is equivalent to the spectrum in the lower panel of Fig. 2 measured at the same frequency (36.1 GHz). In a similar way, the spectrum at $\varphi = 30^\circ$ in Fig. 4 is similar to the spectrum at 36.7 GHz in Fig. 3. Thus, the results in Fig. 4 establish a continuous transformation of spectra in Fig. 2 to the spectra in Fig. 3. These dependencies allow to separate absorption features from different domains.

Fig. 5 shows the angular dependence of the resonance field for the out-of-plane rotation of \mathbf{H} . Solid symbols in the upper panel correspond to experiments with field rotated within the $(\bar{1}10)$ plane. The resonance field ini-

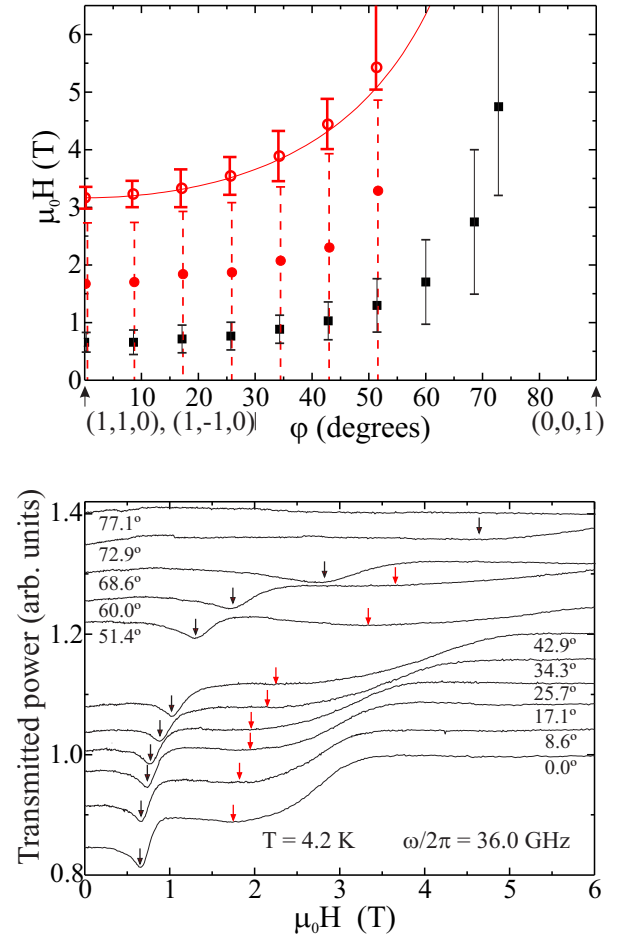


FIG. 5: (color online) Upper panel: (solid symbols) Angular dependencies of the resonance fields for magnetic field rotated within the $(\bar{1}10)$ plane and at $\omega/2\pi = 36.0$ GHz; (open symbols) angular dependencies of H_{res} for the rotation of the magnetic field within (110) plane and at 89.7 GHz. The angles are measured with respect to the trigonal plane. Red symbols correspond to the resonances from the $[110]$ domains, black symbols - from $[100]$ or $[010]$ domains. The error bars mark the line width measured on the half level of the absorbed power. Lower panel: examples of the ESR absorption for different directions of the applied magnetic field. $T = 4.2$ K.

tially increases with increasing angle and for $\varphi > 70^\circ$ rapidly exceeds our experimental field range. Since the frequency in these experiments was near the gap of the low frequency branch (≈ 33 GHz) we can conclude, that for field directions perpendicular to trigonal plane, the low frequency branch is almost independent on H . This fact indicates strong anisotropy along the hexagonal axis in CuCrO_2 .

Similar angular dependencies of the resonance positions were obtained for the field rotated within (110) plane. The corresponding angular dependence of $H_{res}(\varphi)$ at $\omega/2\pi = 89.7$ GHz for the $[110]$ domain is shown in Fig. 5 with red open symbols. We can expect, that for such field rotation and for $H < H_c$ the orientation of

the (110) spin plane does not change. Therefore, in case of strong anisotropy along the hexagonal axis, the resonance field will be defined by the field projection on the hexagonal plane, i.e.: $H_{res} = H_{res}(\varphi = 0) / \cos(\varphi)$. This dependency is given in Fig. 5 with a solid line and agrees well with the experimental points.

The high frequency branch of the ESR spectra in CuCrO_2 was studied using the quasi-optical technique. Transmitted power through the CuCrO_2 single-crystalline platelet at various magnetic fields $\mathbf{H} \parallel [1\bar{1}0]$ are shown in Fig. 6. These frequency dependencies were obtained by division of transmitted power measured at $T = 3$ K by transmitted power measured in the paramagnetic state, $T = 30$ K ($T > T_N$). Such procedure was used to separate the weak signal of the magnetic resonance absorption from other contributions like standing waves within the sample. Fitting of the absorption with Lorenz line shape is shown with a thick solid line. Magnetic field dependencies of the parameters of the observed modes are shown in Fig. 7. The measurements were performed in Voigt geometry with $\mathbf{k} \perp \mu_0 \mathbf{H}$ and at two polarizations of electromagnetic waves: $\mathbf{h} \perp \mathbf{H}$ and $\mathbf{h} \parallel \mathbf{H}$. Here $\mathbf{k} \parallel [001]$ is the wave vector of the electromagnetic radiation.

In the case $\mathbf{h} \perp \mathbf{H}$, as shown in the upper panel of Fig. 6, only the high-frequency mode of the [100] and [010] domains is excited for $H < H_c$. After the spin flop transition for $H > H_c$ the [110] domains are rotated by 90 degrees and they can be excited by the ac field $\mathbf{h} \perp \mathbf{H}$ as well. This explains the increase in the mode intensity in high magnetic fields as observed in the upper panel of Fig. 6 and given as solid circles in the upper panel of Fig. 7.

In the geometry with $\mathbf{h} \parallel \mathbf{H}$ (lower panel of Fig. 6) both [100] and [010] domains are only weakly excited because the excitation conditions are more favorable for [110] domain. In this case the observed signal basically comes from the [110] domains which dominate the spectra. In low magnetic fields the resonance frequency of these domains is practically field-independent (solid triangles in the lower panel of Fig. 7). After the spin flop transition for $H > H_c$ the [110] domains cannot be excited in the geometry $\mathbf{H} \parallel \mathbf{h}$ (see the right inset in Fig. 7). In this case only a weak signal from [100] and [010] domains is observed. This is in agreement with a suppression of the mode intensity as shown in the upper panel of Fig. 7 by solid triangles.

V. BUILDING AND CONTROL OF MAGNETIC DOMAINS IN CuCrO_2

As discussed above, the ESR technique allows to recognize the absorption modes originating from different domains. In this sections we demonstrate that structural and magnetic domains are strongly sensitive to thermal and magnetic history of the sample and that magnetic domains are mobile already at temperatures close to 5 K.

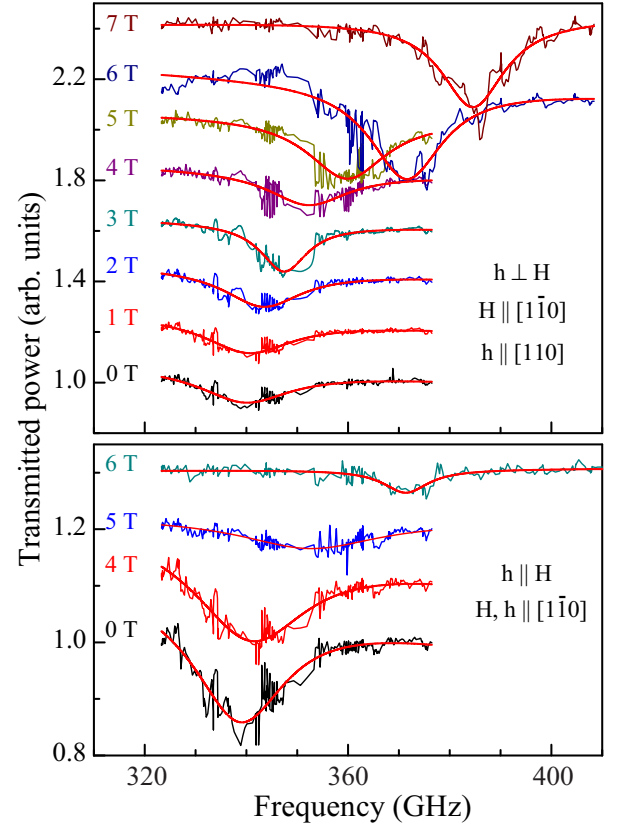


FIG. 6: (color online) Frequency dependence of the transmitted power at different magnetic fields measured in the quasi-optical geometry and for two polarizations of electromagnetic waves: $\mathbf{h} \perp \mathbf{H}$ (upper panel) and $\mathbf{h} \parallel \mathbf{H}$ (lower panel). The radiation propagates along the crystallographic [001] axis and perpendicular to the large plane of the platelet sample. Thick solid lines shows the fits to the spectra using the Lorenz line shape. $T = 3$ K. The orientation of the magnetic domains is shown in Fig. 7.

To obtain the results presented in this chapter we repeated the experiments within the geometry of Fig. 3, i.e. at magnetic fields perpendicular to one side of triangle structure: $\mathbf{H} \parallel [\bar{1}10]$. The data have been obtained at the lowest temperature of our spectrometer $T = 1.2$ K and at two frequencies of 36.1 GHz and 17.1 GHz. As discussed above, within this geometry the spectra at lower frequency show a magnetic mode above critical spin-flop field and they are sensitive to [110] domain only. The spectra at 36.1 GHz show two modes at about 0.5 T and 0.9 T (i.e below the spin-flop field) and they correspond to a signal from [110] and ([100]+[010]) domains, respectively. Therefore, analyzing the intensities of the corresponding modes as a function of magnetic and thermal history, we obtain information about relative population of different domains.

Figs. 8,9 show the ESR spectra measured within the geometry of Fig. 3 but for different magnetic and thermal history of the sample. In the experiments presented in Fig. 8 the sample was cooled in various static magnetic

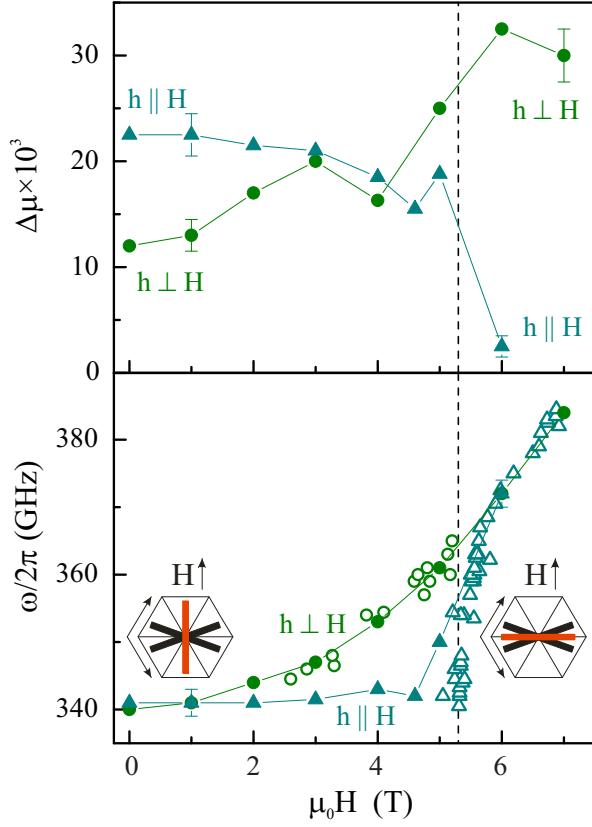


FIG. 7: (color online) Parameters of the high-frequency ESR mode in CuCrO_2 . The data were obtained for two different geometries as indicated: $\mathbf{h} \perp \mathbf{H}$ (circles) and $\mathbf{h} \parallel \mathbf{H}$ (triangles). In both cases the radiation propagates perpendicular to the hexagonal plane and the ac magnetic field \mathbf{h} is within the plane. Upper panel: magnetic contribution, lower panel: resonance positions. Solid symbols were obtained from the frequency scans, open symbols - from the magnetic field scans at a fixed frequency. Solid lines are to guide the eye, dashed line indicates the position of the critical spin-flop field. The insets in the lower panel show the suggested orientation of the magnetic domains below and above H_c . $T = 3$ K.

fields as indicated (field-cooled regime). In the experiments presented in Fig. 9 the mobility of the domains was investigated. The sample was initially cooled down to 1.2 K in zero magnetic field, producing all three domains. In a second step the sample was annealed at various temperatures T_{heat} and at static magnetic field $\mu_0 H_{\text{heat}} = 7.7$ T applied along the $[\bar{1}10]$ direction. Such field annealing lasted two minutes. In a following step first the temperature and then the field were reduced to $T = 1.2$ K and to $H = 0$. Such treatment has been done prior to every field scan shown in Fig. 9.

First, we start the discussion with the results of the field-cooling experiments, which are shown in Fig. 8. The absorption lines measured at 17.5 GHz and attributed to the domains with distorted $[110]$ side are shown on the top panel of Fig. 8. These absorption modes appear at magnetic fields higher the spin-flop field: $H > H_c$.

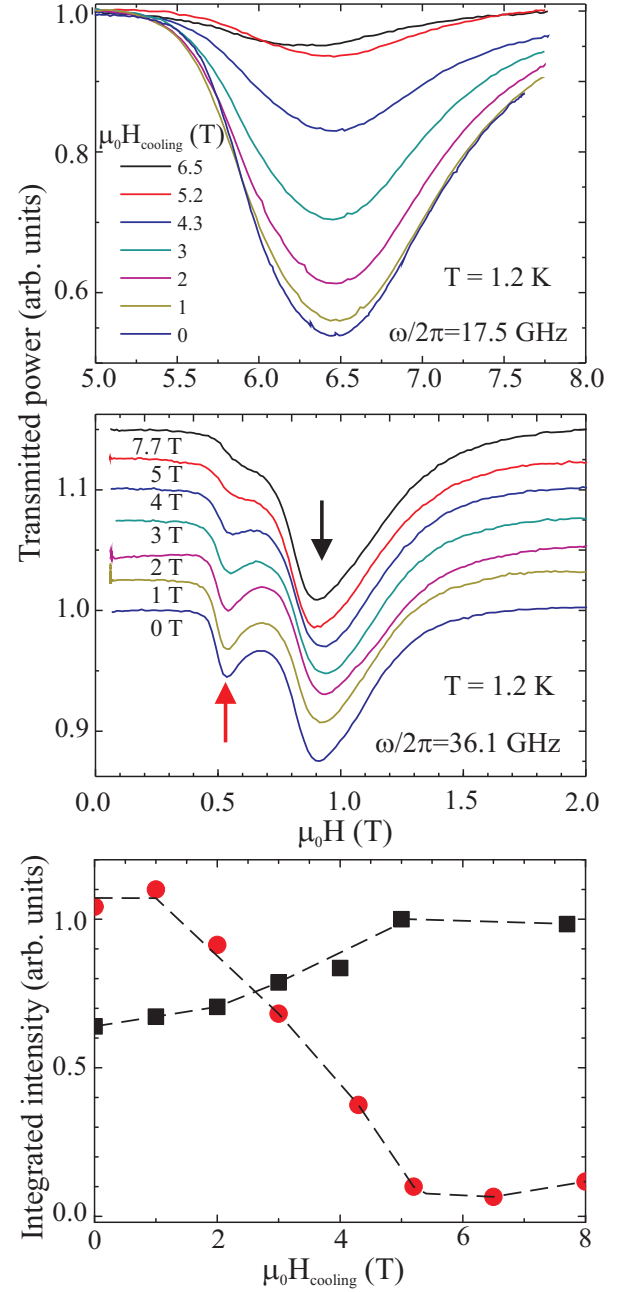


FIG. 8: (color online) ESR absorption lines measured for magnetic field perpendicular to one side of triangular structure ($\mathbf{H} \parallel [\bar{1}10]$) and at $T = 1.2$ K. Top panel: absorption line measured at 17.5 GHz which corresponds to the $[110]$ domains and is seen for $H > H_c$. Middle panel: absorption lines of the $[110]$ domains and $[100]+[010]$ domains measured at 36.1 GHz, marked with red and black arrows respectively. The data were obtained for a field-cooled sample at different fields H_{cooling} . Bottom panel: the integral intensity of the ESR lines as function of H_{cooling} for $[110]$ domain obtained from the curves in the top panel (red circles) and for $[100]+[010]$ domains obtained from the middle panel (black squares). Dotted lines are guides for the eye.

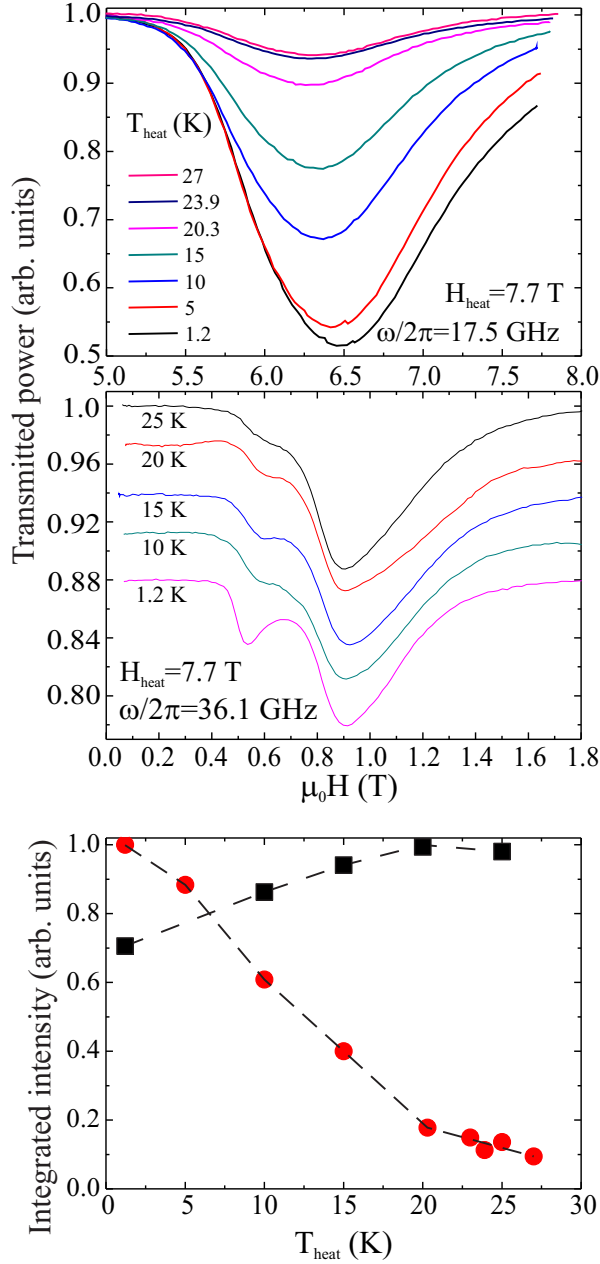


FIG. 9: (color online) ESR absorption lines measured for magnetic field perpendicular to one side of triangular structure ($\mathbf{H} \parallel [\bar{1}10]$) and at $T = 1.2$ K. Top panel: absorption line measured at 17.5 GHz which corresponds to the [110] domains and is seen for $H > H_c$. Middle panel: absorption lines of the [110] domains and [100]+[010] domains measured at 36.1 GHz and marked with red and black arrows respectively. The data were measured after annealing of the sample at different T_{heat} and at $\mu_0 H_{\text{heat}} = 7.7$ T. Bottom panel: the integral intensity of the ESR lines as a function of T_{heat} for the [110] domains obtained from the data of the top panel (red circles) and for [100]+[010] domains obtained from the middle panel (black squares). Dotted lines are guides for the eye.

Clearly, the intensity of the observed mode is strongly suppressed for the field-cooled sample.

The middle panel of Fig. 8 shows the spectra measured at fields below the spin flop transition: $H < H_c$. The mode that is marked by red arrow corresponds to the absorption line from [110] domain and it obviously demonstrates the same behavior as the spectra in the upper panel. In addition, the mode from two other domains, [100] and [010], is observed in these experiments as well. This mode is more intensive in this geometry and it is marked by black arrow. The field cooling reduces the integral intensity of absorption line from the [110] domain and increases the intensity from two other domains. This experiment shows, that a comparatively small external field suppresses the energetically less favorable domain and shifts the ESR intensity to two other domains. This qualitative analysis is supported by the values of integrated intensities of the ESR modes as given in the bottom panel of Fig. 8.

The absorption lines shown in Fig. 9 were obtained using the cooling history as described above. Here the initial zero-field cooling step produces all three domains. In this case, the spectra taken at $T_{\text{heat}} = 1.2$ K in Fig. 9 closely follow the curves with $H_{\text{cooling}} = 0$ in Fig. 8. The subsequent annealing of the zero-field cooled sample in magnetic field results in decrease of the intensity of absorption from energetically not favorable [110] domain and the transfer of the ESR intensity to two other domains. Surprisingly, the domain distribution changes even at $T_{\text{heat}} \ll T_N$. Small change of absorption line intensity was observable even after annealing at $T_{\text{heat}} = 5$ K. The bottom panel of Fig. 9 show the change in the integral intensities of the absorption lines from different domains as a function of annealing temperature.

VI. DISCUSSION

The field and angular dependencies of the resonance frequencies as observed at $T \ll T_N$ in CuCrO_2 can be consistently described by the model of coplanar exchange spin-structure whose orientation in space is defined by weak relativistic interactions with external field and by the crystal environment. The phenomenological hydrodynamical theory of macroscopic dynamics of magnets with dominant exchange interactions was developed in Ref. [20]. The application of this theory to the coplanar magnetic structures was described in Ref. [21] and will be used in the following discussion. The anisotropic part of the energy of magnetic structure of CuCrO_2 can be written as:

$$U = -\frac{\chi_{\parallel} - \chi_{\perp}}{2}(\mathbf{nH})^2 + \frac{1}{2}(An_x^2 + Bn_y^2), \quad (3)$$

where \mathbf{n} is a unit vector perpendicular to the spin plane; χ_{\parallel} and χ_{\perp} are the susceptibilities of the planar structure parallel and perpendicular to \mathbf{n} and they are defined by exchange interactions; A and B are the anisotropy constants. For the case of CuCrO_2 : $\mathbf{z} \parallel [001]$, $\mathbf{y} \parallel [\bar{1}10]$,

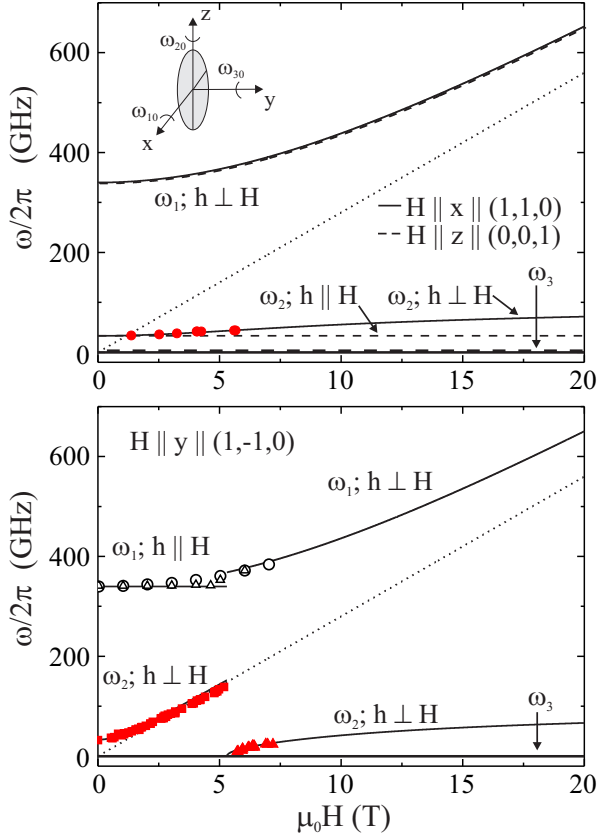


FIG. 10: (color online) Theoretical frequency-field dependences of the ESR modes for field directions $\mathbf{H} \parallel [110]$ and $\mathbf{H} \parallel [\bar{1}10]$. The spectra are computed following Ref. [21] and using three parameters $\omega_{10}/2\pi = 340$ GHz, $\omega_{20}/2\pi = 33$ GHz and $H_{cy} = 5.3$ T. The polarization conditions necessary for the excitation of the ESR are given near the branches. Experimental resonance frequencies $\omega(H_{res})$ for the domains with the distortion of triangular structure along the $[110]$ direction are shown with red solid symbols. Open black symbols show the ESR $\omega_{res}(H)$ obtained from quasi-optical experiments at $\mathbf{h} \perp \mathbf{H}$ (circles) and at $\mathbf{h} \parallel \mathbf{H}$ (triangles). The dotted line corresponds to a paramagnetic mode with $g = 2$.

$\mathbf{x} \parallel [110]$, $A < B < 0$ and $\chi_{\parallel} > \chi_{\perp}$. The minimum of energy at $\mathbf{H} \parallel \mathbf{x}$ is realized for the structure with $\mathbf{n} \parallel \mathbf{x}$. At field directions $\mathbf{H} \parallel \mathbf{z}$ and $\mathbf{H} \parallel \mathbf{y}$ a spin reorientation take place at critical fields $H_{cz}^2 = -A/(\chi_{\parallel} - \chi_{\perp})$ and $H_{cy}^2 = (B - A)/(\chi_{\parallel} - \chi_{\perp})$, respectively. For fields below H_c the spin plane is oriented by crystal anisotropy: $\mathbf{n} \parallel \mathbf{x}$. At $H > H_c$ the spin plane is oriented by field: $\mathbf{n} \parallel \mathbf{H}$. The resonance frequencies of acoustic modes of planar spin structures can be obtained in the frame of Lagrangian formalism²⁰ using the potential energy in form of Eq. (3). The resonance frequencies at zero magnetic field are: $w_{10}^2 = \gamma(-A)/\chi_{\perp}$; $w_{20}^2 = \gamma(B - A)/\chi_{\perp}$, and $w_{30} = 0$, where γ is the gyromagnetic ratio. These frequencies correspond to oscillations of the spin structure around three axes as schematically shown in the inset to Fig. 10. The zero energy oscillation (w_3) indicates the degeneracy of the ground state with respect to rotations

of the structure around the vector \mathbf{n} . The experimental values of $w_{10}/2\pi = 340$ GHz and $w_{20}/2\pi = 33$ GHz and the spin-flop field $H_{cy} = 5.3$ T at $\mathbf{H} \parallel \mathbf{y}$ obtained here are in a good agreement with the results given in Ref. [10].

The values of w_{20} and H_{cy} allow to define the susceptibility anisotropy of the spin structure: $\eta = (\chi_{\parallel} - \chi_{\perp})/\chi_{\perp} = (\omega_{20}/\gamma H_{cy})^2 = 0.045 \pm 0.03$. This small anisotropy is a result of close similarity of the magnetic structure of CuCrO_2 to the regular 2D triangular structure, for which, if we neglect fluctuations, χ_{\parallel} is equal to χ_{\perp} .

From the present results we can evaluate the spin-flop field for $\mathbf{H} \parallel \mathbf{z}$ as: $H_{cz} = H_{cy}(w_{10}/w_{20}) \approx 55$ T. This value exceeds by far our available experimental range, but is still much below the expected saturation field of CuCrO_2 . The latter can be estimated using the susceptibility value $\chi = 0.006$ emu/mol,²² as: $H_{sat} \approx M_{sat}/\chi \approx 650$ T.

Theoretical field dependence of the resonance frequencies for field directions $\mathbf{H} \parallel [110]$ and $\mathbf{H} \parallel [\bar{1}10]$ are shown in Fig. 10. The spectra are defined by three parameters ω_{10} , ω_{20} and H_{cy} as given above. The experimental resonance frequencies for the domain with distortion of triangular structure along $[110]$ direction are shown in the same figure with red symbols. Open black symbols in Fig. 10 show the high frequency excitation branches from all three domains.

The excitation conditions of the magnetic modes are indicated at the theoretical curves in Fig. 10. The high frequency magnetic field \mathbf{h} is directed along the vector ω denoting the corresponding oscillation of the spin plane²⁰. The high frequency branch at $\mathbf{H} \parallel [\bar{1}10]$ and $H < H_{cy}$ can be excited by $\mathbf{h} \parallel \mathbf{H}$ and for $H > H_{cy}$ by $\mathbf{h} \perp \mathbf{H}$. Such polarization excitation conditions agrees well with the present experiment (see Fig. 6).

The experimental study of the magnetic domain distribution in the single crystals of CuCrO_2 shows that their relative size depends on the magnetic history of the sample. The sample cooled at zero magnetic field has three domains of comparable volume. Both, the field cooling and the field annealing reduces the volume of the domains which are oriented unfavorably with respect to static field. The data demonstrates that the rebuilding of the domains takes place at temperatures much below the Néel temperature. Such behavior indicates an anomalously large mobility of magnetic domain walls in CuCrO_2 . The observed effect needs further investigations in order to test the magnetic structure during the rebuilding of the domains. In particular, it is necessary to prove experimentally that the wave vector direction within the domains agrees with the in-plane anisotropy.

We note that for each magnetic domain with a specific orientation of the spin plane two different directions of the chirality vector exist. According to Refs. [9,12] and due to magnetoelectric coupling in CuCrO_2 these magnetic domains can be switched by external electric fields. Such high sensitivity of the magnetic structure in CuCrO_2 to external effects makes this system very at-

tractive from the experimental point of view.

VII. CONCLUSIONS

The results of low temperature ESR experiments in CuCrO_2 are well described in the frame of phenomenological model of coplanar spin structure with biaxial anisotropy. This material is an ideal example of a frustrated triangular quasi-two-dimensional antiferromagnet with spin $S = 3/2$. CuCrO_2 occupies an intermediate position between the systems with large spin which are intensively studied experimentally and theoretically and

the systems with $S = 1/2$, for which the experimental objects are still far from being a model for theory.

Acknowledgments

We thank V. I. Marchenko for useful discussion. This work is supported by Russian Foundation for Basic Research, Program of Russian Scientific Schools (Grants 12-02-00557-a, 10-02-01105-a, 11-02-92707-IND-a, 12-02-31220 mol-a) and by Austrian Science Funds (I815-N16, W1243).

-
- * Electronic address: svistov@kapitza.ras.ru
- ¹ H. Kawamura and S. Miyashita, J. Phys. Soc. Jpn. **54**, 4530 (1985).
 - ² S. E. Korshunov, J. Phys. C: Solid State Phys. **19**, 5927 (1986).
 - ³ P. W. Anderson, Science **235**, 1196 (1987).
 - ⁴ M. L. Plumer, A. Caille, Phys. Rev. B **42**, 10388 (1990).
 - ⁵ A. V. Chubukov and D. I. Golosov, J. Phys.: Condens. Matter **3**, 69 (1991).
 - ⁶ Steven R. W. White and A. L. Chernyshev, Phys. Rev. Lett **99**, 127004 (2007).
 - ⁷ H. Kadowaki, H. Kikuchi and Y. Ajiro J. Phys.: Condens. Matter **2**, 4485-4493 (1990).
 - ⁸ M. Poienar, F. Damay, C. Martin, V. Hardy, A. Maignan, and G. Andre, Phys. Rev. B **79**, 014412 (2009).
 - ⁹ K. Kimura, H. Nakamura, S. Kimura, M. Hagiwara, and T. Kimura, Phys. Rev. Lett. **103**, 107201 (2009).
 - ¹⁰ H. Yamaguchi, S. Ohtomo, S. Kimura, M. Hagiwara, K. Kimura, T. Kimura, T. Okuda, and K. Kindo, Phys. Rev. B **81**, 033104 (2010).
 - ¹¹ B. V. Beznosikov, K. S. Alexandrov, J. Str. Chem. **50**, 108-113 (2009).
 - ¹² K. Kimura, T. Otani, H. Nakamura, Y. Wakabayashi, and T. Kimura, J. Phys. Soc. Jpn. **78**, 113710 (2009).
 - ¹³ M. Frontzek, G. Ehlers, A. Podlesnyak, H. Cao, M. Matsuda, O. Zaharko, N. Aliouane, S. Barilo, S. V. Shiryayev, J. Phys.: Condens. Matter **24**, 016004 (2012).
 - ¹⁴ M. Poienar, F. Damay, C. Martin, J. Robert, and S. Petit, Phys. Rev. B **81**, 104411 (2010).
 - ¹⁵ M. Soda, K. Kimura, T. Kimura, M. Matsuura, K. Hirota, J. Phys. Soc. Jpn. **78**, 124703 (2009).
 - ¹⁶ S. Seki, Y. Onose, and Y. Tokura, Phys. Rev. Lett. **101**, 067204 (2008).
 - ¹⁷ A. A. Volkov, Yu. G. Goncharov, G. V. Kozlov, S. P. Lebedev, and A. M. Prokhorov., Infrared Phys. **25**, 369 (1985).
 - ¹⁸ A. Pimenov, S. Tachos, T. Rudolf, A. Loidl, D. Schrupp, M. Sing, R. Claessen, and V. A. M. Brabers. Phys. Rev. B **72**, 035131 (2005).
 - ¹⁹ D. Ivannikov, M. Biberacher, H.-A. Krug von Nidda, A. Pimenov, A. Loidl, A. A. Mukhin, and A. M. Balbashov. Phys. Rev. B **65**, 214422 (2002).
 - ²⁰ A. F. Andreev and V. I. Marchenko Usp. Fiz. Nauk **130**, 39, (1980).
 - ²¹ L. E. Svistov, L. A. Prozorova, A. M. Farutin, A. A. Gippius, K. S. Okhotnikov, A. A. Bush, K. E. Kamentsev, and É. A. Tishchenko, JETP **135**, 1151 (2009) or see attachment in A.A. Bush, N. Büttgen, A.A. Gippius, V.N. Glazkov, W. Kraetschmer, L.A. Prozorova, L.E. Svistov, A.M. Vasiliev, A. Zheludev and A.M. Farutin, e-print arXiv:1304.4728.
 - ²² K. Kimura, H. Nakamura, K. Ohgushi, and T. Kimura, Phys. Rev. B. **78**, 140401 (2008).